Journal of Power Sources 245 (2014) 730–738

Contents lists available at SciVerse ScienceDirect

Journal of Power Sources

journal homepage: www.elsevier.com/locate/jpowsour

Investigation of a novel ternary electrolyte based on dimethyl sulfite and lithium difluoromono(oxalato)borate for lithium ion batteries

Renjie Chen [a,b,*], Lu Zhu [a], Feng Wu [a,b,**], Li Li [a,b,**], Rong Zhang [a], Shi Chen [a]

[a] School of Chemical Engineering and the Environment, Beijing Institute of Technology, Beijing 100081, China
[b] National Development Center for High Technology Green Materials, Beijing 100081, China

HIGHLIGHTS

- We report a new electrolyte system based on LiODFB and DMS.
- LiODFB–EC/EMC/DMS electrolyte forms a stable SEI film on MCMB electrode.
- The reversible capacity is as high as 222.4 mAh g^{-1} at 1C.

GRAPHICAL ABSTRACT

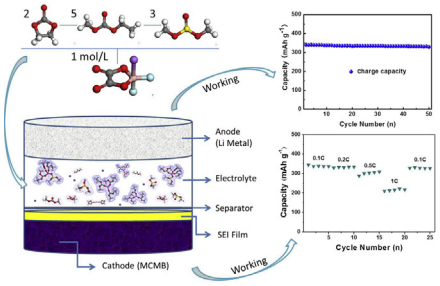

ARTICLE INFO

Article history:
Received 14 December 2012
Received in revised form
29 May 2013
Accepted 21 June 2013
Available online 4 July 2013

Keywords:
Lithium salt
Functional electrolyte
Sulfite
Lithium ion battery

ABSTRACT

Lithium difluoromono(oxalato)borate (LiODFB) has been used as a novel lithium salt for battery in recent studies. In this study, a series of novel electrolytes has been prepared by adding 30 vol% dimethyl sulfite (DMS) or dimethyl carbonate (DMC) as co-solvent into an ethylene carbonate (EC)/ethyl methyl carbonate (EMC) + LiX mixture, in which the LiX could be $LiClO_4$, LiODFB, LiBOB, LiTFSI, or $LiCF_3SO_3$. These ternary electrolytes have been investigated for use in lithium ion batteries. FT-IR spectroscopy analysis shows that characteristic functional groups ($-CO_3$, $-SO_3$) undergo red-shift or blue-shift with the addition of different lithium salts. The LiODFB–EC/EMC/DMS electrolyte exhibits high ionic conductivity, which is mainly because of the low melting point of DMS, and LiODFB possessing high solubility. The Li/MCMB cells containing this novel electrolyte exhibit high capacities, good cycling performance, and excellent rate performance. These performances are probably because both LiODFB and DMS can assist in the formation of SEI films by reductive decomposition. Additionally, the discharge capacity of Li/$LiCoO_2$ half cell containing LiODFB–EC/EMC/DMS electrolyte is 130.9 mAh g^{-1} after 50 cycles, and it is very comparable with the standard-commercial electrolyte. The results show that this study produces a promising electrolyte candidate for lithium ion batteries.

1. Introduction

Lithium ion batteries (LIBs) have attracted significant attention in modern electrochemistry and are widely used in many applications, such as an energy storage device for electric or hybrid electric vehicles. However, lithium ion batteries have increasing safety concerns, such as lithium metal deposition on the graphite anodes which can cause a short circuit and the use of $LiPF_6$ might release HF because of

* Corresponding author. School of Chemical Engineering and the Environment, Beijing Institute of Technology, Beijing 100081, China.
** Corresponding authors. School of Chemical Engineering and the Environment, Beijing Institute of Technology, Beijing 100081, China. Tel.: +86 10 68912508; fax: +86 10 68451429.
E-mail addresses: chenrjbit@sina.com (R. Chen), wufeng863@bit.edu.cn (F. Wu), Lily863@bit.edu.cn (L. Li).

0378-7753/$ – see front matter © 2013 Elsevier B.V. All rights reserved.
http://dx.doi.org/10.1016/j.jpowsour.2013.06.132

its poor thermal stability due to trace moisture. Many studies are focused on increasing the reliability of LIBs [1–8]. Such studies involve examining solid-state electrolytes, shutdown separators, electrolyte additives and flame retardants [9–14].

Electrolytes are often considered key to improving the performance of LIBs. Currently, organic solvents based electrolytes are most commonly used in LIB because of their excellent properties such as high conductivity, low viscosity and high ionic mobility. Most commercial electrolytes are composed of lithium salts, such as $LiPF_6$, and mixed solvents such as ethylene carbonate (EC) and ethyl methyl carbonate (EMC) [15–17]. Cyclic EC has a high dielectric constant, good compatibility with graphite electrodes and it enables the dissolution of lithium salts to sufficient concentrations. However, it is highly viscous and gives poor conductivity even at ambient temperatures. When EC is mixed with linear alkyl carbonates, such as diethyl carbonate (DEC), dimethyl carbonate (DMC), or EMC, more rapid ion transport is achieved as a result of lower viscosity and subsequently higher ionic conductivity is observed [18–20]. The resulting binary or ternary mixed solutions are widely used in commercially available LIBs. The choice of co-solvent is a critical issue that significantly affects not only the conductivity, but also the electrochemical performance, including the physicochemical properties of solid electrolyte interface (SEI) formation [21]. In recent years, sulfites such as dimethyl sulfite (DMS), glycol sulfite (ES), butylene sulfite (BS), and diethyl sulfite (DES) have been studied for use in LIBs as solvents or additives because of their good properties, such as their film-forming abilities [22–25].

Lithium difluoromono(oxalato)borate (LiODFB) is one of the most promising lithium salts available for use in LIBs. LiODFB-based electrolytes have several unique characteristics which include ideal ionic conductivity over a wide temperature range. They would be able to support LIBs operating at high temperatures and can deliver high capacity at low temperatures with high current rates. They also provide increased protection against operation under abused conditions. These electrolytes are able to form and stabilize SEI films on the surface of graphite electrodes [25–30]. It is also known that LiODFB is more soluble in linear carbonate solvents than LiBOB and the LIBs using LiODFB has a better capability and cycle performance at low temperature [31].

In this study, ternary electrolyte systems based on various lithium salts (lithium perchlorate ($LiClO_4$), lithium trifluoromethanesulfonate ($LiCF_3SO_3$), lithium bis(trifluoromethanesulfone) imide (LiTFSI), lithium bis(oxalato)borate (LiBOB), lithium difluoromono(oxalato)borate (LiODFB)) and organic carbonate solvents, such as EC and EMC, were prepared with co-solvents DMC or DMS. Their physicochemical properties and electrochemical performances were evaluated using galvanostatic charge–discharge tests, electrochemical impedance spectroscopy (EIS), cyclic voltammetry (CV) measurements and energy dispersive spectrometry (EDS) tests. Fourier transform infrared (ATR-FTIR) analysis was applied to comprehensively study the chemical structure of the electrolytes. It was found that using DMS as a co-solvent with the lithium salt, LiODFB, resulted in an excellent electrolyte candidate for use in lithium ion batteries.

2. Experimental

Lithium salts, $LiClO_4$ (AP, Acros), LiBOB (>99.9%), $LiCF_3SO_3$ (AP, Acros), LiTFSI (99%, 3 M), and LiODFB (>99.9%) were dried at 140 °C for 12 h under vacuum. DMS (AP. 98%, Acros) was used as received. Organic compounds such as EC (AP. 99%), EMC (AP. 98%), DMC (AP. 99%) are illustrated in Scheme 1.

All electrolyte systems were prepared by dissolving each lithium salt of ($LiClO_4$, LiBOB, $LiCF_3SO_3$, LiTFSI, LiODFB) in organic solvents to make two series of electrolytes (with and without DMS; EC:EMC:DMC = 2:3:5 by volume, EC:EMC:DMS = 2:3:5 by volume) in an argon-filled MBraun LabMaster 130 glove box (H_2O < 5 ppm). All lithium salts were used at a concentration of 1 mol L^{-1} except for LiBOB (0.6 M) because of its lower solubility in organic solvents [32]. The reference electrolyte was 1 M $LiPF_6$ dissolved in EC and DMC (1:1 by volume). The IR spectra of the samples, which were placed on the ATR unit in the glove box, were recorded on a NICOLET6700 spectrometer at 4000 cm^{-1}–400 cm^{-1} in Ar atmosphere, and the spectral resolution was set at 2 cm^{-1}. Ionic conductivity measurements were carried out in an electrochemical cell with Pt electrodes. The cell constant was determined with a standard KCl solution (0.01 M) at 25 °C. The alternating current impedances of the samples were measured using a CHI604D electrochemical workstation (1 Hz–100 kHz, −40 to 90 °C, Shanghai Chenhua Company, Shanghai, China). Cells were assembled in a glove box. Thermal behavior was investigated using a differential scanning calorimeter (DSC, MDSC 2910, TA Instruments, USA). Samples of ~10 mg were sealed in aluminum pans and transferred into the DSC sample holder. The pans were cooled to −100 °C by liquid nitrogen and then heated to 100 °C at a rate of 10 °C min^{-1} under N_2. The calculations were set with the DMol3 module of module of the Cerius2 program. The molecular structure of the organic carbonates (EC, EMC, DMC) and sulfite (DMS) were optimized using the BLYP function of nonlocal DFT with DNP group. The energies of the frontier molecular orbitals were also calculated using this program.

The graphite electrode is composed of 80 wt.% graphitized mesocarbon microbeads (MCMB), 10 wt.% acetylene black, and 10 wt.% polyvinylidene fluoride (PVDF). The slurry was coated on to copper foils, then dried under vacuum at 80 °C for 12 h and cut to 8 mm × 8 mm in size. The $LiCoO_2$ electrodes were similarly prepared. Li/MCMB and Li/$LiCoO_2$ button cells (CR 2025) were assembled in the argon-filled glove box, and the electrodes were separated by a polypropylene film (Celgard® 2400, North Carolina, USA). All electrodes were soaked with LiX–EC/EMC/DMC or LiX–EC/EMC/DMS electrolyte. The cyclic voltammetry (CV) measurements of the batteries were performed on a CHI604D electrochemical workstation with a scan rate of 0.1 mV s^{-1} at room temperature. The samples for scanning electron microscopy (SEM) and energy dispersive spectrometry (EDS) tests were washed with DMC, and they were dried at 80 °C for 12 h. SEM was tested by a HITACHI S-3500N and EDS was measured during acquisition of SEM photographs. The galvanostatic charge–discharge tests were carried out on a Land Cell tester (CT2001A, Wuhan Jinnuo Company, China) at room temperature. For Li/MCMB cells, the operation voltages were set at 2 V and 0.005 V, and for Li/$LiCoO_2$ cells, the operation voltages were set at 4.2 V and 2.7 V.

3. Results and discussion

3.1. ATR-FTIR analysis

The ATR-FTIR is a useful tool to analyze the interactions between cations and anions in electrolytes. The ATR-FTIR spectra in Fig. 1 shows the ν(C–O–C) and ν(C=O) stretching vibrations of the organic compounds in the LiX–EC/EMC/DMC electrolyte systems. In Fig. 1(a), the half peak width gradually increases and the peak moves to the high frequency region (blue shift) when LiX is introduced into the electrolyte. This is resulted of that the electron cloud density of O atom of C–O–C band is more negatively than that of C atoms. Then the Li^+ ions could easily coordinate with the O atom. With the stretching vibrations of C–O–C being affected by the interactions between Li^+ ions and O atoms, the blue shifts occur. The C–O–C stretching band is shifted from 1256 cm^{-1} [33] to 1264 cm^{-1} with added LiODFB. According to Scheme 1, we can clearly see that there is a $-CO_3$ group in the structure of carbonate. The C atom's *sp*2 hybridized orbital consist of three bands between

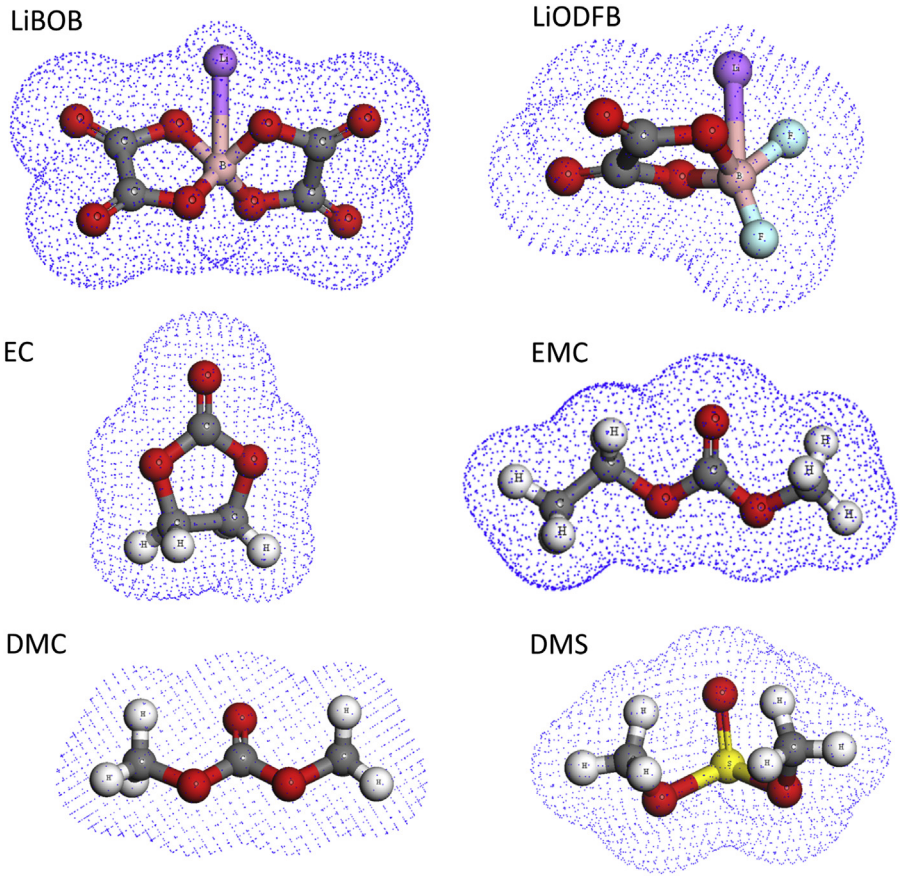

Scheme 1. Structures of part of lithium salts and organic dissolvents.

C atom and O atoms (C═O band and two O–C bands). The electron cloud density of carbonyl oxygen is the largest among $-CO_3$, which contributes to the coordination with 2s empty orbit of Li^+ ions. So carbonyl oxygen has a strong coordination with Li^+ ions. The C═O band stretching vibration mainly lies in three bands [33]: (1) C═O stretching vibration of the chain carbonate (such as EMC or DMC) at 1750 cm^{-1}, (2) C═O symmetric stretching vibration of EC from 1810 cm^{-1} to 1725 cm^{-1}, (3) harmonic peaks caused by Fermi resonance at 1806 cm^{-1}. In Fig. 1(b), where the concentration of Li^+ ions is sufficiently high, the peak (1775 cm^{-1}) increases in size but has no shift. The harmonic peak (1806 cm^{-1}) moves to a lower wave number (red shift). It can be concluded that Li^+ ions coordinated with the C═O band affected this stretching vibration. This coordination causes the C═O bonds to lengthen and the bond strength to become weaker, leading to the red shift.

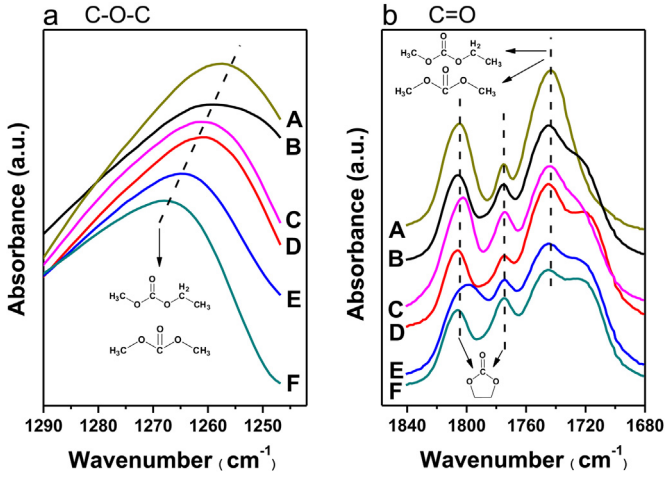

Fig. 1. ATR-FTIR spectra of the ν(C–O–C) stretching mode (a) and the C═O stretching mode (b) of the electrolytes LiX–EC/EMC/DMC A: EC/EMC/DMC; B: $LiCF_3SO_3$–EC/EMC/DMC; C: LiBOB–EC/EMC/DMC; D: $LiClO_4$–EC/EMC/DMC; E: LiODFB–EC/EMC/DMC; F: LiTFSI–EC/EMC/DMC.

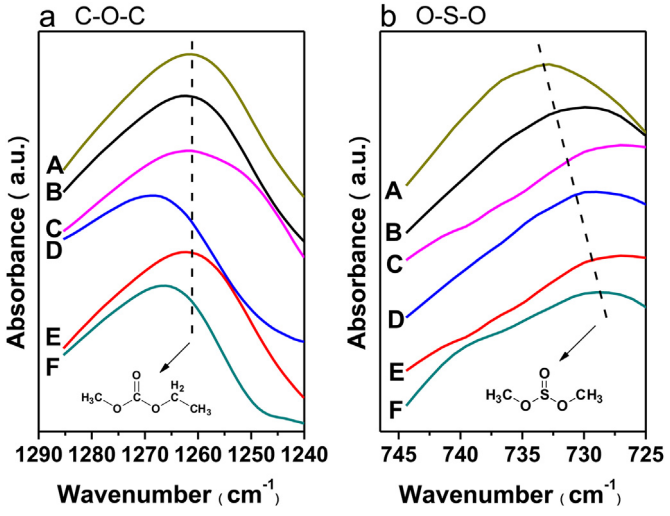

Fig. 2. ATR-FTIR spectra of the C–O–C stretching mode (a), the O–S–O stretching mode (b) of the electrolyte systems LiX–EC/EMC/DMS. A: EC/EMC/DMS; B: $LiCF_3SO_3$–EC/EMC/DMS; C: LiBOB–EC/EMC/DMS; D: $LiClO_4$–EC/EMC/DMS; E: LiODFB–EC/EMC/DMS; F: LiTFSI–EC/EMC/DMS.

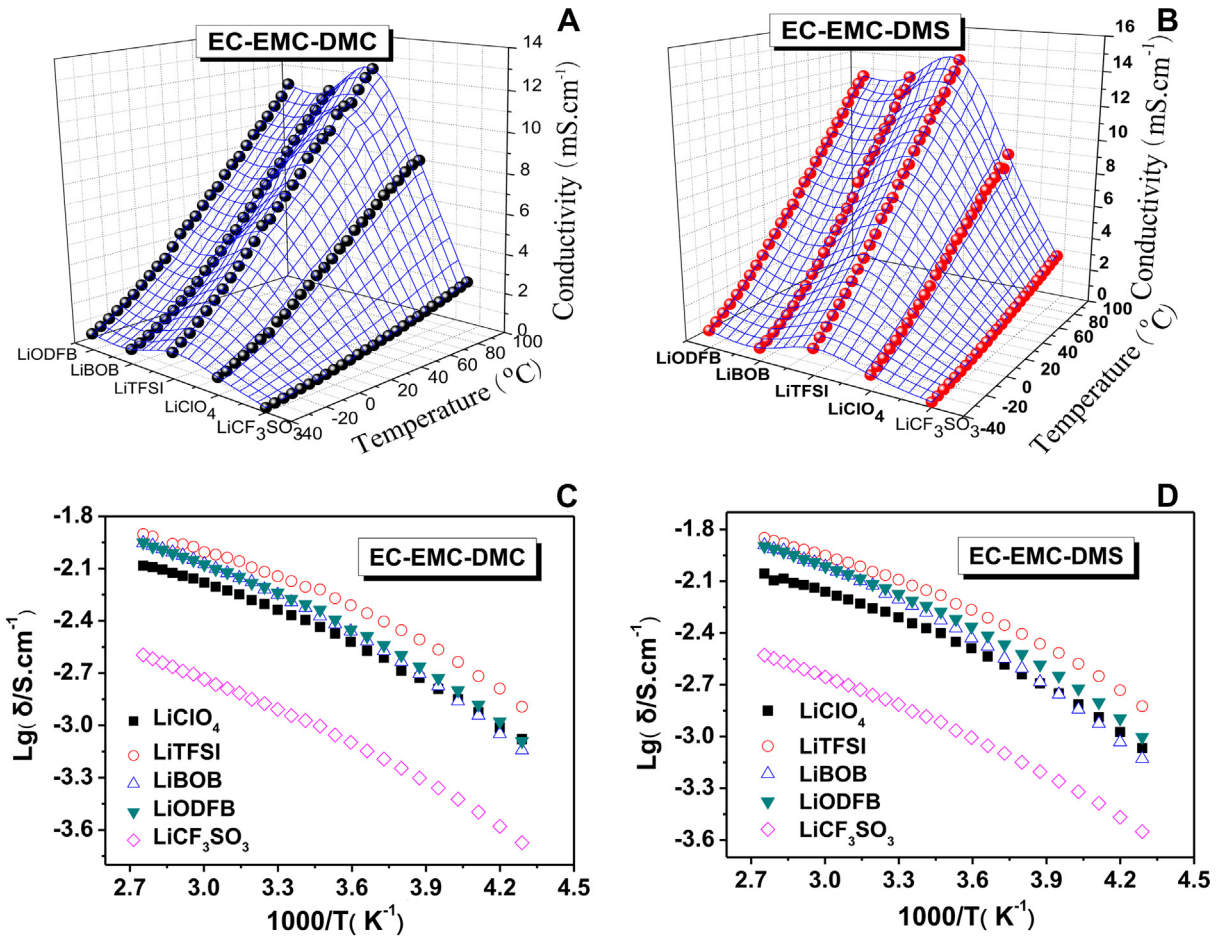

Fig. 3. The relationships between conductivity with different lithium salt in LiX–EC/EMC/DMC (A) and LiX–EC/EMC/DMS (B) at various temperatures. Arrhenius plots of LiX–EC/EMC/DMC (C) and LiX–EC/EMC/DMS (D).

Fig. 2 spectra shows the *v*(C–O–C) and *v*(O–S–O) stretching vibrations from the organic compounds in the LiX–EC/EMC/DMS electrolyte systems. The C–O–C peak strength is reduced while the half peak width gradually increases, with the peak blue shifted to the high frequency region. The C–O–C stretching band shifts from 1260 cm^{-1} to 1266 cm^{-1} with added LiODFB. The degree of solvation of Li^+ ions varies for different lithium salts. Because of the sulfur atom's *sp*3 hybridized orbital structure for sulfite-based electrolytes, Li^+ ions interact with the oxygen in pentagons of O–S–O.

In Fig. 2(b), the O–S–O peak is red shifted to lower frequencies. The O atoms in the O–S–O band are affected by Li^+ ion, which is reflected in the infrared spectroscopy where the O–S–O peaks move to a lower wave number. The O–S–O stretching band shifts from 732 cm^{-1} [33] to 728 cm^{-1} when LiODFB is added. The opposite behavior of C–O–C and O–S–O (blue shift for C–O–C but red shift for O–S–O) is because of the structure of DMS molecule. The relative electronegativity of $-SO_3$ group is stronger than that of $-CO_3$ group [22]. Li^+ ions strongly coordinate with S=O band, and the electron clouds density of O atoms in O–S–O band are affected. Consequently, the O–S–O peak red shifts to lower frequencies. Figs. 1 and 2 show the relationship between lithium-ion solvation and the radius of lithium salt anion in these systems, and DMS affects the solvation between lithium salts and other solvents. These changes indicate that intension of interactions between

Table 1
Ionic conductivities and melting points for electrolytes with different lithium salt and different organic compounds at various temperatures (10^{-3} S cm^{-1}).

Organic compounds	Lithium salt	Conductivity (10^{-3} S cm^{-1})							Melting point (°C)
		−40 °C	20 °C	0 °C	25 °C	40 °C	60 °C	90 °C	
EC/EMC/DMC (2:5:3)	$LiClO_4$	0.83	1.62	2.68	4.29	5.24	6.7	8.24	−67.67
	$LiCF_3SO_3$	0.21	0.437	0.71	1.14	1.41	1.84	2.54	−64.67
	LiTFSI	1.28	2.72	4.4	6.73	8.08	9.86	12.52	−72.92
	LiBOB	0.72	1.68	3.04	5.1	6.65	8.44	11.14	−66.6
	LiODFB	0.81	1.87	3.25	5.31	6.57	8.39	11.21	−68.88
EC/EMC/DMS (2:5:3)	$LiClO_4$	0.95	1.78	3.23	5.03	6.15	7.68	9.78	−71.52
	$LiCF_3SO_3$	0.28	0.55	0.98	1.4	1.74	2.21	2.96	−69.89
	LiTFSI	1.5	3.05	4.88	7.5	9.03	11.17	14.17	−71.2
	LiBOB	0.74	1.75	3.32	5.73	7.52	9.67	12.87	−70.66
	LiODFB	0.99	2.25	3.84	6.12	7.63	9.69	12.66	−69.01

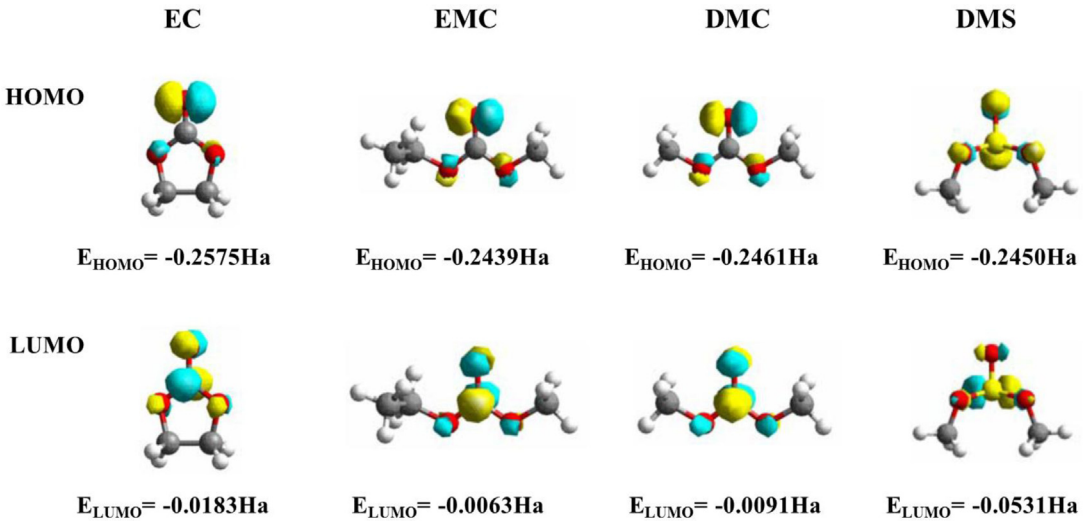

Fig. 4. Molecular orbitals of EC, EMC, DMC and DMS, and their energies.

lithium salts and solvents molecules differs, and these electrolyte systems would probably show different performances such as different ion conductivities.

3.2. Electrochemical evaluation

The relationship between the conductivity and different lithium salts in LiX–EC/EMC/DMC and LiX–EC/EMC/DMS electrolyte systems at various temperatures is shown in Fig. 3(A) and (B). In the observed temperature range (−40°C to 90 °C), the ionic conductivity increases with the temperature. Even at −40 °C, all samples were able to achieve an ion conductivity of 10^{-4} S cm^{-1}. In Fig. 3, the LiTFSI based electrolytes show the highest ionic conductivities at room temperature (6.73×10^{-3} S cm^{-1} at 25 °C for LiTFSI–EC/EMC/DMC, 7.5×10^{-3} S cm^{-1} for LiTFSI–EC/EMC/DMS), as summarized in Table 1. These results also show that the ionic conductivity of LiX–EC/EMC/DMS is higher than that of LiX–EC/EMC/DMC at each tested temperature. This can be attributed to the lower viscosity of DMS than DMC because a relatively low viscosity, which results in a low activation energy for Li^+ ion diffusion, would improve the conductivity of electrolyte solution. The results support the hypothesis that sulfites can improve the performance of carbonates at low temperatures, giving improved parameters such as higher ionic conductivity. Subsequently, it can be recommended that DMS based LIB can be applied over a wider temperature range. Fig. 3(C) and (D) shows the Arrhenius plots of all the ternary systems over a temperature range of −40 °C to 90 °C. The Arrhenius plots of ionic conductivity for each electrolyte protrude upwards, indicating that for these electrolytes, the conductivity and temperature relation does not follow the Arrhenius equation. Conductivity increases due to the decrease in viscosity. The melting points of these electrolytes were investigated by DSC and are shown in Table 1. All melting points were found to be below −65 °C. For LiX–EC/EMC/DMC systems, the sequence of melting points for the lithium salts can be ranked as LiTFSI < LiODFB < $LiClO_4$ < LiBOB < $LiCF_3SO_3$. For every lithium salt, the melting point of DMS based electrolytes is lower than those that are DMC based, while the ionic conductivity is higher. This demonstrates that DMS co-solvent electrolytes maintain good physicochemical properties even at very low temperatures.

The energy separation, E_g, of the lowest unoccupied molecular orbital (LUMO) and the highest occupied molecular orbital (HOMO) determine the ability of molecules to lose and gain electrons [22] and the electrochemical stability of the electrolyte [32]. The molecular orbitals of HOMO and LUMO for EC, EMC, DMC, and DMS are given in Fig. 4 and the frontier molecular orbital energies are listed in Table 2. The LUMO energy and the total energy of the DMS molecule are lower than the related energies for carbonate molecules, and based on the molecular orbital theory, the molecules for organic DMS can easily accept electrons and remain stable even with a high reaction activity. It indicates that the reductive decomposition of DMS molecules is likely to occur during the forming of SEI film. And this indicates that the electrolyte with DMS may show some better performances than the electrolyte without DMS.

Table 2
Total energy, frontier molecular orbital energy EC, EMC, DMC and DMS molecules.

Organic molecule	Frontier molecular orbital energy (Ha)		
	E_{HOMO}	E_{LUMO}	ΔE_g^a
Ethylene carbonate (EC)	−0.2575	−0.0183	0.2392
Ethyl methyl carbonate (EMC)	−0.2439	−0.0063	0.2376
Dimethyl carbonate (DMC)	−0.2461	−0.0091	0.2370
Dimethyl sulfite (DMS)	−0.2450	−0.0531	0.1919

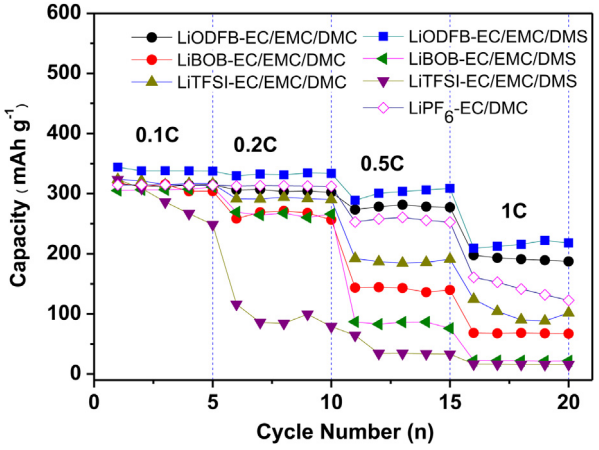

Fig. 5. Cycle performance with different rates of Li/MCMB cells containing LiODFB–EC/EMC/DMC, LiBOB–EC/EMC/DMC, LiTFSI–EC/EMC/DMC, LiODFB–EC/EMC/DMS, LiBOB–EC/EMC/DMS, LiTFSI–EC/EMC/DMS and LPF_6–EC/DMC electrolytes.

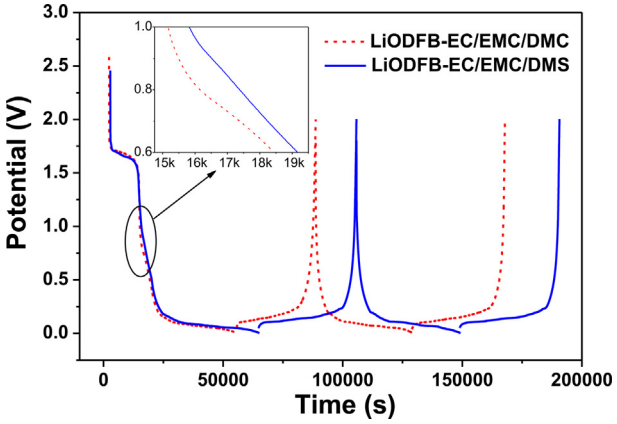

Fig. 6. The charge/discharge curves for Li/MCMB cells containing LiODFB–EC/EMC/DMC and LiODFB–EC/EMC/DMS as electrolyte (i = 0.1 mA, cut off at 2.00/0.005 V vs. Li/Li$^+$).

3.3. Charge–discharge tests

As discussed above in Section 3.2, LiTFSI–EC/EMC/(DMC or DMS) based electrolytes have a higher conductivity than LiODFB–EC/EMC/(DMC or DMS) based electrolytes. It has been shown that LiODFB can help to form a stable film on the electrode in former studies [34]. However, LiTFSI was found to cause corrosion on aluminum current collectors. Hence, LiODFB–EC/EMC/(DMC or DMS) based electrolytes were selected to be used for the cells with MCMB cathodes and lithium anodes.

Table 3
The reversible capacities for Li/MCMB cells containing different electrolytes.

Electrolyte	Reversible capacity (mAh g^{-1})		
	2nd cycle	25th cycle	50th cycle
LiODFB–EC/EMC/DMC	299.6	283.6	259.7
LiODFB–EC/EMC/DMS	339.7	333.9	329.0
LiPF$_6$–EC/DMC	300.2	302.1	300.5

The rate capacity versus cycle performance of Li/MCMB cells containing LiX(LiTFSI/LiBOB/LiODFB)–EC/EMC/DMC, LiX(LiTFSI/LiBOB/LiODFB)–EC/EMC/DMS and LiPF$_6$–EC/DMC electrolytes is illustrated in Fig. 5. This shows that the novel electrolyte containing LiODFB–EC/EMC/DMS had the best cycle and rate performance, with LiODFB–EC/EMC/DMC being second in rate performance. For commercial electrolyte, the cycle performance at low rate (0.1C, 0.2C) is better than that of LiODFB–EC/EMC/DMC electrolyte. But with the increasing of the current density, the capacity of Li/MCMB cell containing LiPF$_6$–EC/DMC is lower than Li/MCMB cells containing LiODFB–EC/EMC/DMS or LiODFB–EC/EMC/DMC electrolyte. This can be contributed to the unique characteristics of LiODFB [25] and indicates that there is an effective SEI film formed and located on the surface of MCMB electrodes when LiODFB is used.

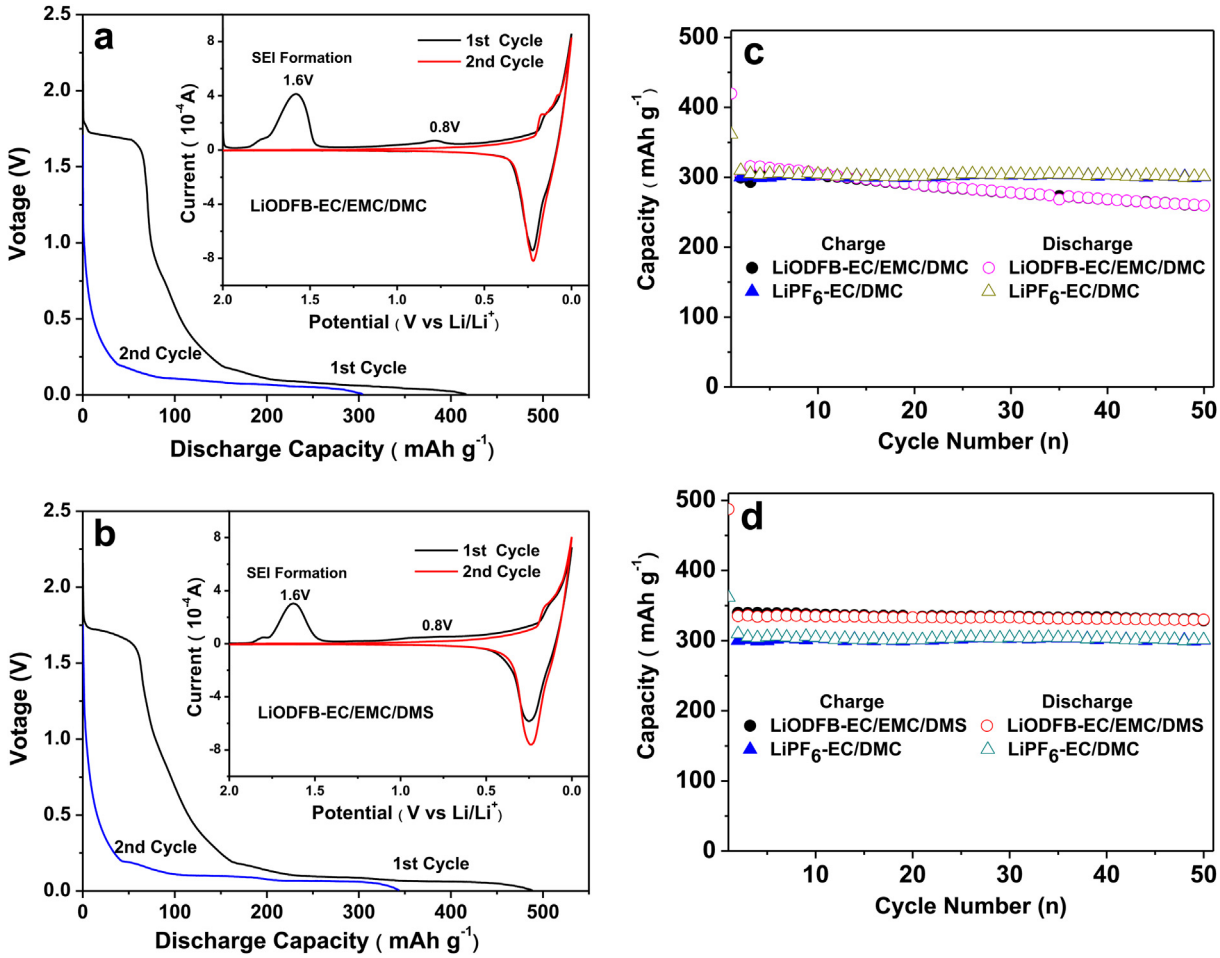

Fig. 7. The first and second discharge cycles (charge–discharge current is 0.1C) of Li/MCMB cells containing: (a) LiODFB–EC/EMC/DMC, (b) LiODFB–EC/EMC/DMS; and the insets show the CV curves of these Li/MCMB cells (2–0 V with a scan rate of 0.1 mV s^{-1}). Charge–discharge curves of Li/MCMB cells containing (c) LiODFB–EC/EMC/DMC and LiPF$_6$–EC/DMC electrolyte, (d) LiODFB–EC/EMC/DMS and LiPF$_6$–EC/DMC electrolyte. The insets show the coulombic efficiencies of the Li/MCMB cells. The charge–discharge current is 0.1C.

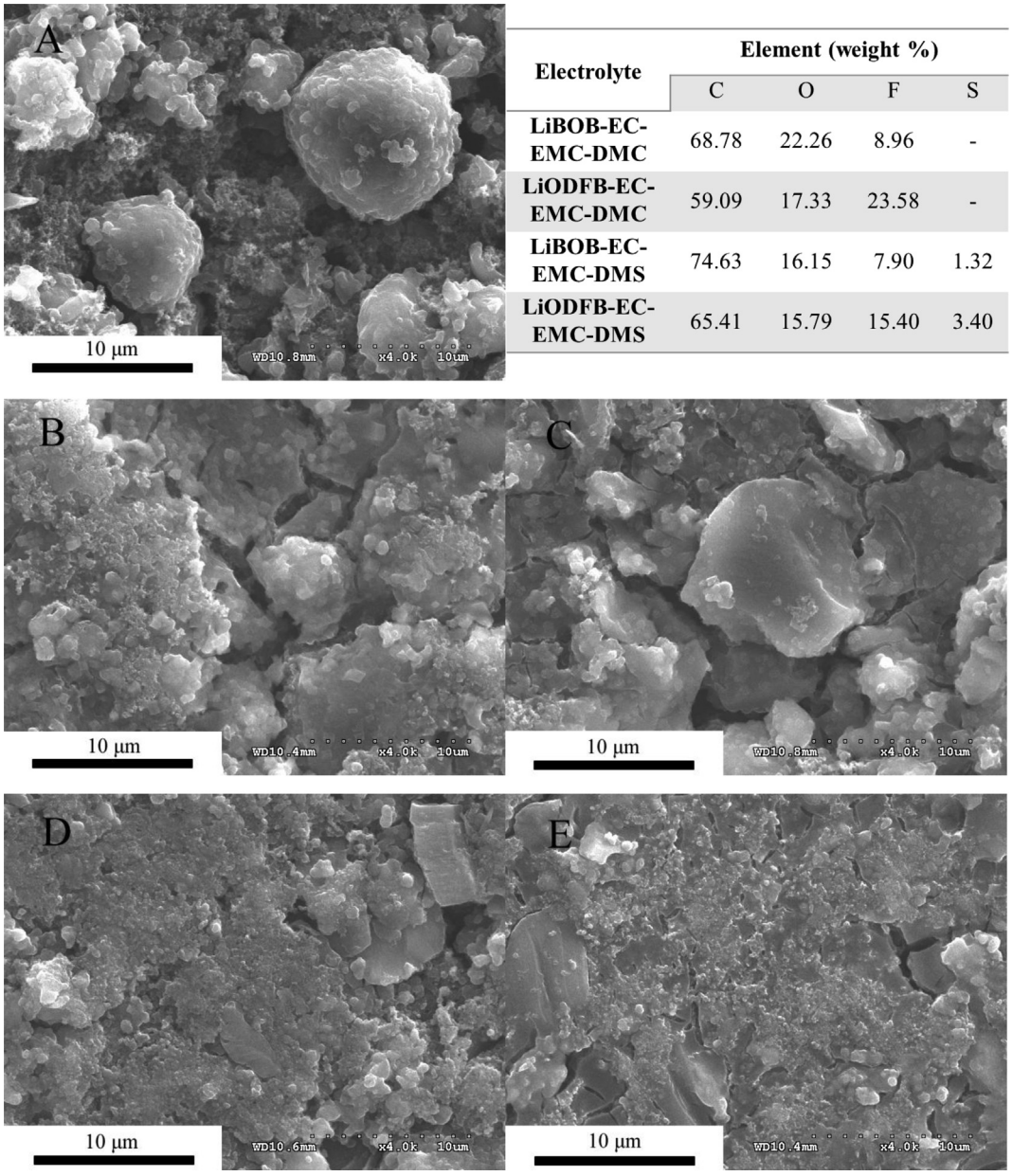

Electrolyte	Element (weight %)			
	C	O	F	S
LiBOB-EC-EMC-DMC	68.78	22.26	8.96	-
LiODFB-EC-EMC-DMC	59.09	17.33	23.58	-
LiBOB-EC-EMC-DMS	74.63	16.15	7.90	1.32
LiODFB-EC-EMC-DMS	65.41	15.79	15.40	3.40

Fig. 8. SEM photographs of MCMB electrodes after cycling with different electrolytes and the content of elements of the electrodes tests by EDS (because the content of B is so little that it can't achieve to the detection limit and can't be measured.) A: MCMB; B: LiBOB–EC/EMC/DMC; C: LiODFB–EC/EMC/DMC; D: LiBOB–EC/EMC/DMS; E: LiODFB–EC/EMC/DMS.

According to these results, LiODFB is the most promising lithium salt studied in this paper. LiODFB will be the focus of subsequent works. To investigate the capacity performance of novel electrolytes, galvanostatic charge–discharge tests between 2.0 V and 0.005 V were carried out as shown in Fig. 6. The discharging plateau shown around 1.6 V indicates the decomposition process of LiODFB and the formation of a solid electrolyte interface (SEI) on the surface of the MCMBs. DMS and DMC also decomposed in the discharge process. DMS decomposed at ~1.6 V, near the plateau of LiODFB. The electrochemical reactions of carbonates DMC and EC caused plateaus at ~0.8 V, shown in Fig. 6 (inset). In the second cycle, the plateau is caused by the intercalation of lithium, shown as the only plateau. This indicates that the SEI film has formed. To clarify the more clearly, the initial two voltage-discharge curves of Li/MCMB cells with electrolytes containing DMC or DMS are shown in Fig. 7(a) and (b). Corresponding to Fig. 6, there are different plateaus in the first cycle of the cells. The intercalation of Li^+ ions observed blow 0.3 V. Around 1.6 V the electrochemical reactions occur to form SEI film, and the reduction of ODFB anions and solvent molecules such as DMS lengthen the first plateau stages. In the second curve, there is only one plateau which is caused by the intercalation of Li^+ ions. This confirms that the formation of SEI film on the MCMB electrode surface was done through the first charge–discharge cycle. The cyclic voltammetry curves of Li/MCMB cells are also shown in Fig. 7 (insets of a, b). Cyclic voltammetry was studied to clarify the SEI film formation process in greater detail. This shows that there is an irreversible reduction peak near 1.6 V, which reflects the reduction of LiODFB and DMS on the surface of the MCMB. In the second cycle, the peak at 1.6 V disappears. This indicates that the formation of the SEI film has completed. These results coincide with previous discussions in Section 3.3. The peak at 1.6 V for DMC based electrolytes has a larger area than that of DMS based

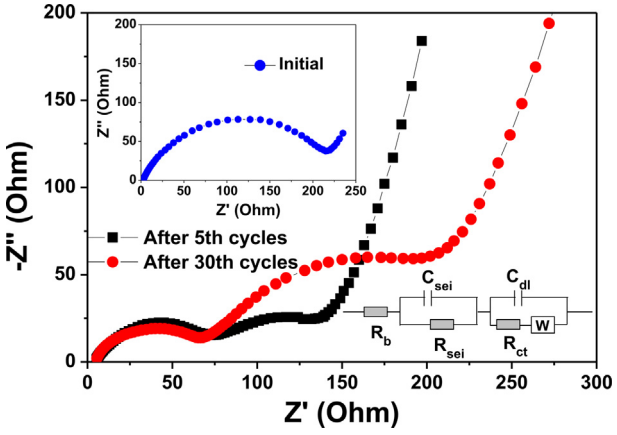

Fig. 9. The EIS of Li/MCMB cell containing LiODFB–EC/EMC/DMS electrolyte in original statement before and after cycling.

electrolytes, which indicates that more DMC molecules take part in the electrochemical reaction on the surface of the MCMB electrode. There is a small peak at 0.8 V attributed to the LiODFB–EC/EMC/DMS electrolyte which is less obvious than the LiODFB–EC/EMC/DMC electrolyte. This indicates that the LiODFB–EC/EMC/DMS electrolyte forms a more stable SEI film at 1.6 V than the LiODFB–EC/EMC/DMC electrolyte. The charge–discharge capacity curves of the Li/MCMB cells with LiODFB–EC/EMC/DMC and LiODFB–EC/EMC/DMS as electrolytes are shown in Fig. 7. By comparing these curves and data in Table 3, it can be determined that the reversible capacity of the LiODFB–EC/EMC/DMS system is higher than that of the LiODFB–EC/EMC/DMC and $LiPF_6$–EC/DMC systems. It can also be inferred that DMS and LiODFB produce more stable SEI films and improve the cycling performances of the batteries. The electrochemical performance of graphite electrodes is improved from the decomposition products of LiODFB and DMS. The charge capacity of the Li/MCMB cell at the 50th cycle is 329.9 mAh g^{-1} (Fig. 7(d)). But for DMC based electrolyte, it reduces to 259.7 mAh g^{-1} (Fig. 7(c)), which can be assigned to the reduction process of DMC. And the charge capacity of the cell containing commercial electrolyte $LiPF_6$–EC/DMC is 300.5 mAh g^{-1} at the 50th cycle. This result sustains that the LiODFB–EC/EMC/DMS electrolyte system could form a stable SEI film on the surface of MCMB electrode again. Sulfites are subsequently better choices to form SEI films than carbonates. According to the LUMO energy of DMS (−0.0531 Ha), DMS is more easily reduced than EC, EMC and DMC. The electrochemical reaction of DMS products deposited on the electrode assist in forming more stable SEI films, enhancing the specific capacity and improving the cycling performance of batteries. Simultaneously, this proves that the lithium salt, LiODFB, forms a robust protective SEI film on the graphite surface.

The SEM and EDS analysis of the SEI film is shown in Fig. 8. In Fig. 8(A), the particles of the initial MCMB electrode are clearly visible. The surface morphologies change with cycling in the electrolyte systems. A compact film is formed on the surface of the MCMB particles. The chemical components of the film are determined by EDS and are given in the table shown in Fig. 8. This shows that the LiODFB–EC/EMC/DMS system forms a much thicker and more compact film than the other systems, and indicates that a lithium-oxy-sulfite film is produced, which could improve the electrochemical performance of graphite electrode. Because of the film forming characteristics of LiBOB, after cycling, the LiBOB–EC/EMC/DMS system also forms a thick SEI film on the surface of the MCMB electrode.

EIS tests of the Li/MCMB cell were performed at room temperature with the LiODFB–EC/EMC/DMS electrolyte, which is in a lithiated state in different cycles. These results are shown in Fig. 9. The impedance spectra show that the original system has a higher interfacial impedance than the samples after cycling. The first semicircle in the high frequency range represents the impedance of the SEI film (R_{sei}) [31]. As shown in Fig. 9, the impedance of the first semicircle in the high frequency range is almost invariable even after 30 cycles. Therefore, the SEI film can be determined as stable. This indicates that the LiODFB–EC/EMC/DMS electrolyte may contribute to better battery performance, improving cycle life and

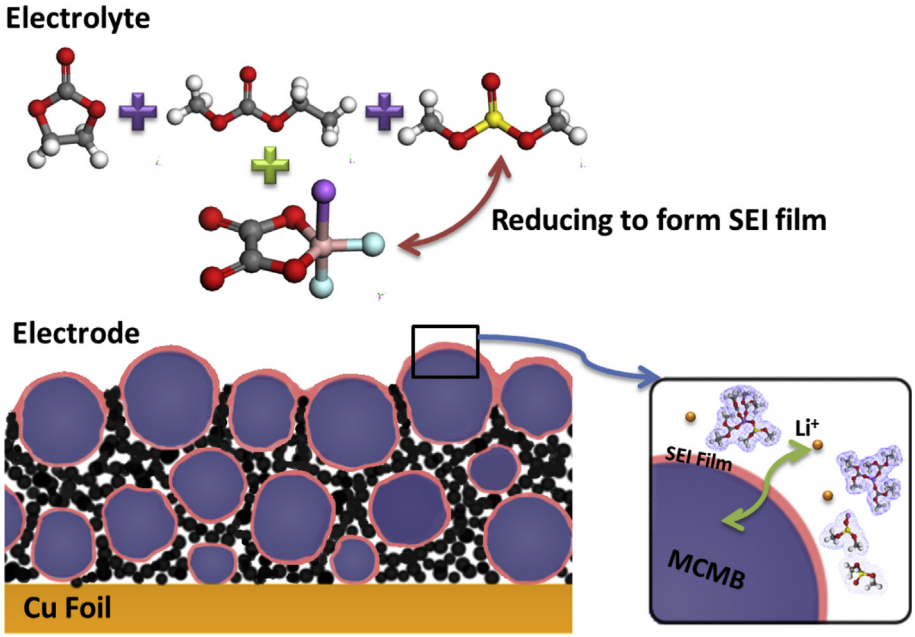

Scheme 2. Schematic illustration of the MCMB electrode after cycling with LiODFB–EC/EMC/DMS electrolyte.

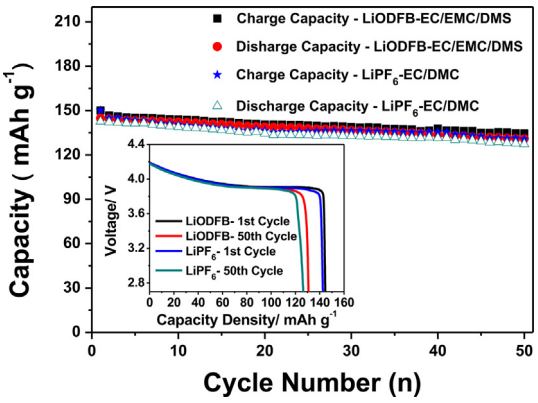

Fig. 10. Charge–discharge capacities of Li/$LiCoO_2$ half cells containing LiODFB–EC/EMC/DMS electrolyte and $LiPF_6$–EC/DMC electrolyte. The inset indicates the discharge profiles of the cells after the 1st and 50th cycles.

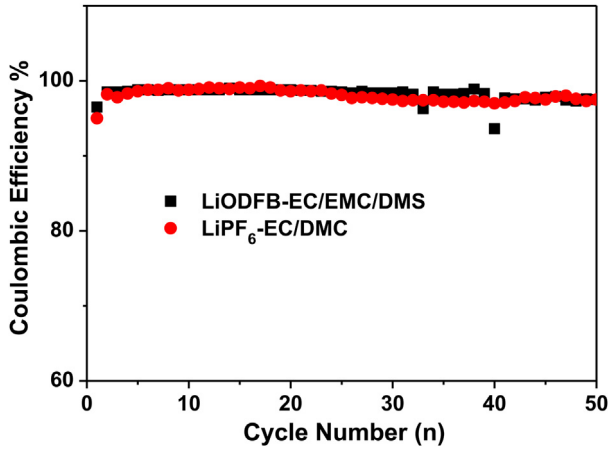

Fig. 11. Coulombic efficiencies of the cells containing LiODFB–EC/EMC/DMS and $LiPF_6$–EC/DMC electrolytes.

rate performance. Scheme 2 shows the schematic illustration of the MCMB electrode cycling with the LiODFB–EC/EMC/DMS electrolyte as applied in this study. As it shows, the reduction of electrolyte on the surface of MCMB particles at the first discharge progress of Li/MCMB cell forms the SEI film to protect graphite from being co-intercalation of solvent molecules between the graphite layers. And only the Li^+ ions are allowed to going through the SEI film.

As shown in Fig. 10, the discharge capacity of the Li/$LiCoO_2$ half-cell containing LiODFB–EC/EMC/DMS electrolyte is 130.9 mAh g^{-1} and the columbic efficiency is 97.5% (Fig. 11) after 50 cycles. The discharge capacity after 50 cycles retains approximately 90.4% of the initial capacity. In contrast, the discharge capacity of the cell which contains $LiPF_6$–EC/DMC electrolyte is a little bit lower than the former one. Its discharge capacity is 127.3 mAh g^{-1}, which is about 89.3% of the initial capacity, and the columbic efficiency is also 97.5%. This indicates that this new kind of electrolyte could be compatible with commercially positive electrode material, $LiCoO_2$, for applications in LIBs.

4. Conclusion

A series of novel ternary LiX–EC/EMC/DMC and LiX–EC/EMC/DMS electrolytes have been prepared and characterized. These ternary electrolytes are stable liquids at room temperature. Because of the addition of lithium salts, LiX, the characteristic peaks of the EC/EMC/DMC and EC/EMC/DMS functional groups were red-shifted or blue-shifted in the FTIR spectra. Lithium salt LiODFB and organic sulfite DMS, show good characteristics, forming a stable solid electrolyte interface through CV tests and charge–discharge analysis. In this study, the electrolyte LiODFB–EC/EMC/DMS shows good electrochemical properties, such as high ionic conductivity (up to 6.12×10^{-3} S cm^{-1} at 25 °C), over a wide range of temperatures. Comparing with commercial electrolyte and LiODFB–EC/EMC/DMC electrolyte, LiODFB–EC/EMC/DMS system shows higher charge/discharge capacity and better rate performance when used in Li/MCMB cells. This novel electrolyte also shows good compatibility with $LiCoO_2$ electrodes. In summary, the results indicate that DMS is an appropriate co-solvent to improve the electrochemical performance of LiODFB. And LiODFB–EC/EMC/DMS organic liquid system is a promising candidate electrolyte for advanced LIBs.

Acknowledgments

This study was supported by the National Key Program for Basic Research of China (No. 2009CB220100), the International S&T Cooperation Program of China (2010DFB63370), the National 863 Program (2011AA11A256), New Century Educational Talents Plan of Chinese Education Ministry (NCET-10-0038) and Beijing Novel Program (2010B018).

References

[1] Z. Zhang, D. Fouchard, J.R. Rea, J. Power Sources 70 (1998) 16–20.
[2] A. Ohta, H. Koshina, H. Okuno, H. Mural, J. Power Sources 54 (1995) 6–10.
[3] K. Kumai, H. Miyashiro, Y. Kobayashi, K. Takei, R. Ishikawa, J. Power Sources 81–82 (1999) 715–719.
[4] S. Tobishima, K. Takei, Y. Sakurai, J. Yamaki, J. Power Sources 90 (2000) 188–195.
[5] N. Yabuuchi, T. Ohzuku, J. Power Sources 119–121 (2003) 171–174.
[6] R. Spotnitz, J. Franklin, J. Power Sources 113 (2003) 81–100.
[7] K.H. Lee, E.H. Song, J.Y. Lee, B.H. Jung, H.S. Lim, J. Power Sources 132 (2004) 201–205.
[8] T. Yamauchi, K. Mizushima, Y. Satoh, S. Yamada, J. Power Sources 136 (2004) 99–107.
[9] F. Wu, G. Tan, R. Chen, L. Li, J. Xiang, Y. Zheng, Adv. Mater. 23 (2011) 5081–5085.
[10] C. Masquelier, Nat. Mater. 10 (2011) 649–650.
[11] Y.S. Kim, T.H. Kim, H. Lee, H.K. Song, Energy Environ. Sci. 4 (2011) 4038–4045.
[12] H.Y. Lee, J.K. Baek, S.M. Lee, H.K. Park, K.Y. Lee, M.H. Kim, J. Power Sources 128 (2004) 61–66.
[13] B.G. Dixon, R.S. Morris, S. Dallek, J. Power Sources 138 (2004) 274–276.
[14] G. Nagasubramanian, C.J. Orendorff, J. Power Sources 196 (2011) 8604–8609.
[15] G.G. Botte, R.E. White, Z. Zhang, J. Power Sources 97–98 (2001) 570–575.
[16] A. Nyman, M. Behm, G. Lindbergh, Electrochim. Acta 53 (2008) 6356–6365.
[17] F. Zhou, X.M. Zhao, J.R. Dahn, Electrochem. Commun. 11 (2009) 589–591.
[18] T. Kawamura, A. Kimura, M. Egashira, S. Okada, J.I. Yamaki, J. Power Sources 104 (2002) 260–264.
[19] S.K. Jeong, M. Inaba, Y. Iriyama, T. Abe, Z. Ogumi, Electrochim. Acta 47 (2002) 1975–1982.
[20] H.Q. Gao, Y.Q. Lai, Z.A. Zhang, Y.X. Liu, Acta Phys. Chim. Sin. 25 (2009) 905–910.
[21] J. Huang, B. Yu, F. Li, W. Qiu, Int. J. Miner. Met. Mater. 16 (2009) 463–467.
[22] R. Chen, F. Wu, L. Li, Y. Guan, X. Qiu, S. Chen, Y. Li, S. Wu, J. Power Sources 172 (2007) 395–403.
[23] L. Xing, W. Li, M. Xu, T. Li, L. Zhou, J. Power Sources 196 (2011) 7044–7047.
[24] S. Li, B. Li, X. Xu, X. Shi, Y. Zhao, L. Mao, X. Cui, J. Power Sources 209 (2012) 295–300.
[25] S.S. Zhang, Electrochem. Commun. 8 (2006) 1423–1428.
[26] V. Aravindan, P. Vickraman, Solid State Sci. 9 (2007) 1069–1073.
[27] V. Aravindan, P. Vickraman, K. Krishnaraj, Polym. Int. 57 (2008) 932–938.
[28] D.P. Abraham, M.M. Furczon, S.-H. Kang, D.W. Dees, A.N. Jansen, J. Power Sources 180 (2008) 612–620.
[29] S.S. Zhang, J. Power Sources 162 (2006) 1379–1394.
[30] J. Liu, Z.H. Chen, S. Bushing, K. Amine, Electrochem. Commun. 9 (2007) 475–479.
[31] S.S. Zhang, J. Power Sources 163 (2007) 713–718.
[32] J.B. Goodenough, Y. Kim, Chem. Mater. 22 (2010) 587–603.
[33] J. Wu, The Technology and Applications of Modern Fourier Transform Infrared Spectroscopy, first ed., vol. 1, Scientific and Technical Documentation Press, Beijing, 1994.
[34] S. Li, X. Xu, X. Shi, B. Li, Y. Zhao, H. Zhang, Y. Li, W. Zhao, X. Cui, L. Mao, J. Power Sources 217 (2012) 503–508.